

Integral representation and its applications in earthquake mechanics: a review

Shiro Hirano

Abstract In seismology, a faulting process as a source is linked with an elastic wavefield as an observable not only via a partial differential equation (PDE) but also via an integral equation. We conduct a review of these links and focus on the latter in terms of forward/inverse analyses of kinematic/dynamic modeling, which are investigated by many seismologists. Difficulties in the analyses are also mentioned: estimation and hyper-singularity of an integration kernel, determination of the number of parameters for modeling, and assumed dynamic friction on faults.

1 Introduction

Earthquake faulting processes are modeled under a framework of dynamic fracture mechanics, which relates rupture extension to displacement/stress perturbations. The faulting processes feature 1) extension of a shear crack under compressive states, 2) rupture velocity up to the speeds of Rayleigh waves, shear waves, or rarely, compressional waves, and 3) balancing with friction of shear traction acting on a slipping surface, etc. We here offer a brief overview of analyses of faulting processes in seismology. We especially focus on an integral representation of dynamic rupture, which is equivalent to a time-dependent double layer potential. The representation was first developed in the frequency domain[27] and subsequently rewritten in the time domain[10]. Finally, Keiichi Aki completed it in a book[3, 4]. As mentioned in this article, the representation has been applied to seismic wavefield simulations (Section 3.1), inverse analyses of fault slip evolution (Section 3.2), and earthquake rupture simulations (Section 3.4). It has also been applied for inverse analyses of co-seismic stress change on faults, although this has only been done in a few studies (Section 3.3).

Shiro Hirano

College of Science and Engineering, Ritsumeikan University, 1-1-1, Noji-Higashi, Kusatsu-city, Shiga, 525-8577, Japan. See <https://interfacial.jp/> for contact details.

2 Formulation

2.1 In Terms of PDE

We start from the equilibrium condition of an elastic body. Let the domain Ω ($\subset \mathbb{R}^3$) be the elastic body (e.g., the Earth) including a bounded surface Γ ($\subset \Omega$) that represents an earthquake fault. Just before an earthquake, we assume that the elastic body is under the equilibrium condition, represented as

$$\nabla \cdot \boldsymbol{\sigma}_0(\mathbf{x}) = 0, \quad \mathbf{x} \in \Omega \quad (1)$$

where $\boldsymbol{\sigma}_0$ is an initial stress tensor in Ω . In this state, $\boldsymbol{\sigma}$ cannot be correlated with displacement or strain of Ω 's interior because the Earth had undergone continuous displacement and had no reference state of the displacement or strain. Thus, when eq. (1) is satisfied, we set a reference for the displacement and strain. Next, let $u_n(\mathbf{x}, t)$ be the n -th component of the displacement vector $\mathbf{u}(\mathbf{x}, t)$ ($\in \mathbb{R}^3$) at the position \mathbf{x} ($\in \Omega \setminus \Gamma$) and time t (≥ 0). As noted above, we assume that the displacement vector field had zero initial conditions: $\mathbf{u} = \partial_t \mathbf{u} = 0$ for $t = 0$. As in fig. 1a, The stress perturbation tensor $\boldsymbol{\sigma}$ in Ω and normal and tangential (i.e., shear) components of the traction perturbation \mathbf{N} and \mathbf{T} , respectively, at $\boldsymbol{\xi}$ ($\in \Gamma$) are defined as

$$\boldsymbol{\sigma}(\mathbf{x}, t) = \frac{1}{2} \mathbf{C}(\mathbf{x}) \left\{ \nabla \mathbf{u}(\mathbf{x}, t) + (\nabla \mathbf{u}(\mathbf{x}, t))^T \right\}, \quad (2)$$

$$\mathbf{N}(\boldsymbol{\xi}, t) = \lim_{\mathbf{x} \rightarrow \boldsymbol{\xi}} \left\{ \mathbf{v}^\Gamma(\boldsymbol{\xi}) \cdot \boldsymbol{\sigma}(\mathbf{x}, t) \mathbf{v}^\Gamma(\boldsymbol{\xi}) \right\} \mathbf{v}^\Gamma(\boldsymbol{\xi}), \quad (3)$$

$$\mathbf{T}(\boldsymbol{\xi}, t) = \lim_{\mathbf{x} \rightarrow \boldsymbol{\xi}} \left\{ \boldsymbol{\sigma}(\mathbf{x}, t) \mathbf{v}^\Gamma(\boldsymbol{\xi}) - \mathbf{N}(\boldsymbol{\xi}, t) \right\}, \quad (4)$$

where $\mathbf{C} = (c_{ijkl})$ is a fourth-order elasticity tensor, and \mathbf{v}^Γ is a local unit normal vector to Γ . Note that \mathbf{N} and \mathbf{T} are independent of the direction of the approach of \mathbf{x} to $\boldsymbol{\xi}$ because of continuity of traction for any surfaces embedded in elastic bodies. Then, our concern is the following PDE and initial/boundary conditions for the displacement and stress perturbations:

$$\begin{cases} \rho(\mathbf{x}) \partial_t^2 \mathbf{u}(\mathbf{x}, t) = \nabla \cdot \boldsymbol{\sigma}(\mathbf{x}, t), & \mathbf{x} \in \Omega \setminus \Gamma, t \geq 0 & (5a) \\ \mathbf{u}(\mathbf{x}, 0) = \partial_t \mathbf{u}(\mathbf{x}, 0) = 0, & \mathbf{x} \in \Omega \setminus \Gamma, & (5b) \\ \boldsymbol{\sigma}(\mathbf{x}, t) \mathbf{v}^{\partial\Omega}(\mathbf{x}) = 0, & \mathbf{x} \in \partial\Omega & (5c) \end{cases}$$

where $\mathbf{v}^{\partial\Omega}$ is a local unit normal vector to $\partial\Omega$. Moreover, one of the following boundary conditions on the fault Γ is required at $\boldsymbol{\xi} \in \Gamma$ and $t \geq 0$:

$$\begin{cases} \lim_{\varepsilon \rightarrow 0} [\mathbf{u}(\boldsymbol{\xi} + \varepsilon \mathbf{v}^\Gamma(\boldsymbol{\xi}), t) - \mathbf{u}(\boldsymbol{\xi} - \varepsilon \mathbf{v}^\Gamma(\boldsymbol{\xi}), t)] = [\mathbf{u}](\boldsymbol{\xi}, t), & (6a) \\ \mathbf{T}_0(\boldsymbol{\xi}) + \mathbf{T}(\boldsymbol{\xi}, t) = \mathbf{f}(\boldsymbol{\xi}, t), & (6b) \end{cases}$$

where \mathbf{T}_0 , obtained by replacing $\boldsymbol{\sigma}$ in eq. (4) by $\boldsymbol{\sigma}_0$, is the background level of the tangential traction, and \mathbf{f} is friction acting on the sliding surface Γ . In the right-hand side of (6a), $[\mathbf{u}]$ is the discontinuity of the displacement field (Fig.1b). For earthquake faulting, we assume non-opening and non-penetration conditions represented as $[\mathbf{u}] \cdot \boldsymbol{\nu}^\Gamma = 0$ because the fault is under a highly compressive state; thus we regard $[\mathbf{u}]$ as slip. A boundary of the support of $[\mathbf{u}]$ is regarded as a rupture front, and its propagation velocity is the rupture velocity. In this regard, analyses of rupture propagation are included in analyses of $[\mathbf{u}]$.

2.2 In Terms of Integral Equation

In seismology, the essential idea is to relate the slip and displacement/stress perturbation at arbitrary points. The following equation is called the representation theorem of Aki & Richards[3, 4]:

$$\mathbf{u}(\mathbf{x}, t) = \int_{\Gamma} \mathbf{m} * \nabla_{\boldsymbol{\xi}} \mathbf{G} d\boldsymbol{\xi} = \int_{\Gamma} \left\{ \int_0^t \mathbf{m}(\boldsymbol{\xi}, \tau) \nabla_{\boldsymbol{\xi}} \mathbf{G}(\mathbf{x}, \boldsymbol{\xi}, t - \tau) d\tau \right\} d\boldsymbol{\xi}, \quad (7)$$

or, with summation convention,

$$u_n(\mathbf{x}, t) = \int_{\Gamma} m_{kl} * \partial_{\xi_l} G_{nk} d\boldsymbol{\xi}, \quad (8)$$

$$m_{kl}(\boldsymbol{\xi}, \tau) = [u_i](\boldsymbol{\xi}, \tau) v_j(\boldsymbol{\xi}) c_{ijkl}(\boldsymbol{\xi}) \quad (9)$$

where the asterisk $*$ denotes a convolution with respect to time from 0 to t , and the contracted tensor $\mathbf{m}(\boldsymbol{\xi}, t)$ defined in eq.(9) is called the seismic moment density tensor or, hereinafter, moment tensor. In eqs. (7) and (8), the second-order Green tensor $\mathbf{G}(\mathbf{x}, \boldsymbol{\xi}, t)$ is the solution to the following problem in Ω :

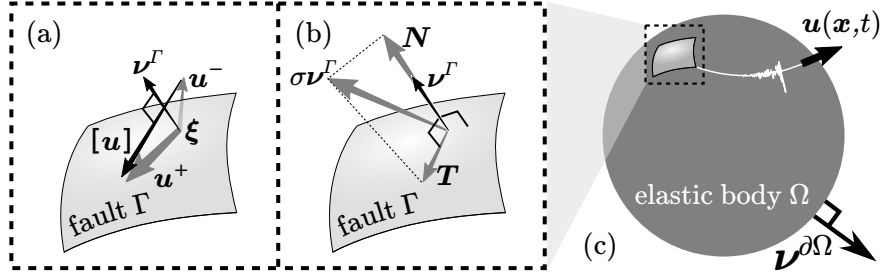


Fig. 1 Schematic illustrations of (a) slip $[\mathbf{u}] := \mathbf{u}^+ - \mathbf{u}^-$ parallel to the fault surface Γ embedded in the elastic body Ω , where \mathbf{u}^+ and \mathbf{u}^- are displacement above and beyond $\boldsymbol{\xi} \in \Gamma$, respectively, and (b) the normal component \mathbf{N} and tangential component \mathbf{T} of the traction perturbation $\boldsymbol{\sigma} \boldsymbol{\nu}^\Gamma$ due to the slip. (c) $\mathbf{u}(\mathbf{x}, t)$ is off-fault displacement due to the seismic wavefield.

$$\left\{ \begin{array}{ll} \rho(\mathbf{x})\partial_t^2 G_{in}(\mathbf{x}, \boldsymbol{\xi}, t) \\ \quad = \partial_{x_j} \{c_{ijkl}(\mathbf{x})\partial_{x_l} G_{kn}(\mathbf{x}, \boldsymbol{\xi}, t)\} + \delta_{in}\delta(\mathbf{x} - \boldsymbol{\xi}, t), & \mathbf{x} \in \Omega, t \geq 0, (10a) \\ G_{nk}(\mathbf{x}, \boldsymbol{\xi}, 0) = \partial_t G_{nk}(\mathbf{x}, \boldsymbol{\xi}, 0) = 0, & \mathbf{x} \in \Omega \setminus \{\boldsymbol{\xi}\}, (10b) \\ c_{ijkl}(\mathbf{x})\nu_j^{\partial\Omega}(\mathbf{x})\partial_{\xi_i} G_{kn}(\mathbf{x}, \boldsymbol{\xi}, t) = 0, & \mathbf{x} \in \partial\Omega, (10c) \end{array} \right.$$

where δ_{in} is Kronecker's delta, and $\delta(\mathbf{x} - \boldsymbol{\xi}, t)$ is Dirac's delta function. Note that \mathbf{x} and $\boldsymbol{\xi}$ in eqs.(10a)–(10c) are taken as arbitrary points in Ω . Hence, eqs.(10a)–(10c) hold in an intact elastic body without the fault surface Γ . In other words, \mathbf{G} is independent of Γ . Thanks to this nature, we can calculate \mathbf{G} even if we do not know all faults embedded in the Earth.

Some advantages of the use of eq.(7) in comparison with finite difference methods (FDMs) and finite element methods (FEMs) are the following. In eq.(7), we consider quantities defined only on Γ to obtain the displacement at \mathbf{x} while FDMs and FEMs require any information all over Ω . Hence, the integral representation requires very few numerically discretized elements. Moreover, when we consider traction on Γ on the basis of eqs.(2)–(4), the boundary integral consists of the traction and moment tensor on Γ in an exact sense. On the other hand, in FDM or FEM, those quantities are sometimes not defined strictly along the fault surface but defined at different points each other in a staggered grid FDM or traditional FEM. Hence, use of eq.(7) has an advantage in view of numerical accuracy and contributes to some analyses in seismology as follows.

3 Practical Problems

3.1 Kinematic Forward Analysis of Seismic Wavefield: $m \mapsto \mathbf{u}$

Calculations of seismic wavefields are an important topic in terms of both geophysics and hazard assessment. Forward simulations of the wavefield are equivalent to solving eqs.(5a)–(5c) with eq.(6a). In many cases, these simulations have been performed using FDMs or FEMs with assumed spatio-temporal distributions of the moment tensor called scenario earthquakes, which are based on past earthquakes analyzed throughout the steps in Section 3.2, or on forward simulations shown in Section 3.4. By using seismometer networks, the near-surface seismic wavefield is directly observable in the aftermath of major earthquakes, allowing researchers to validate the results of their simulations by comparing calculated $\mathbf{u}(\mathbf{x}, t)$ at $\mathbf{x} \in \partial\Omega$ and the observed waveforms. Because this procedure is independent of force, traction, stress, and friction, this is a kinematic modeling of the seismic wavefield.

In principle, the simulations can be executed using eq.(7) if the kernel $\nabla_{\boldsymbol{\xi}} \mathbf{G}$ is available. In particular, reflection, refraction, scattering, and the intrinsic attenuation due to the heterogeneity of the Earth's interior are out of the scope for fundamental understanding on characteristics of seismic radiation from a faulting process. For this purpose, the kernel for an infinite homogeneous isotropic space has been em-

ployed. While the complete form of the kernel can be found in eqs.(4.29)–(4.33) of Aki & Richards[4], the following approximation holds in the far field[12, 3, 4]:

$$\partial_{\xi_i} G_{nk} \sim \frac{\gamma_n \gamma_k \gamma_l}{4\pi\rho c_d^3} \frac{\partial_t \delta\left(t - \frac{r}{c_d}\right)}{r} - \left(\frac{\gamma_n \gamma_k - \delta_{nk}}{4\pi\rho c_s^3}\right) \gamma_l \frac{\partial_t \delta\left(t - \frac{r}{c_s}\right)}{r}, \quad (11)$$

where $\gamma_i = (x_i - \xi_i)/r$, $r = |\mathbf{x} - \boldsymbol{\xi}|$, and c_d and c_s are the speeds of dilatational (i.e., longitudinal or primary) and shear (i.e., transverse or secondary) waves, respectively. Using this kernel and the characteristics of a circular crack model, the spectra of far-field radiation have been studied analytically (e.g., [32, 25]) and numerically (e.g., [25, 23]). Moreover, Hok & Fukuyama[17] executed numerical calculations of ground motion considering a free surface, which is represented using the kernel for the infinite medium. Although the free surface was completely flat in their simulation, their method is applicable to any surface topography. Hence, their method will be applied to more scenario earthquakes for hazard assessment.

For more realistic simulations, a kernel that reflects the heterogeneity of the Earth is required. One powerful tool to obtain it is called an empirical Green's function method[21], as follows. Time-derivative of eq.(7) results in

$$\partial_t \mathbf{u}(\mathbf{x}, t) = \int_{\Gamma} \partial_{\tau} \mathbf{m} * \nabla_{\boldsymbol{\xi}} \mathbf{G} d\boldsymbol{\xi}. \quad (12)$$

This means that, if a support of $\partial_{\tau} \mathbf{m}$ is sufficiently small in space and time (i.e., $\partial_{\tau} \mathbf{m}$ is pulse-like), we may assume that $\partial_{\tau} \mathbf{m} \sim \delta(\boldsymbol{\xi})\delta(\tau)$ holds. Therefore, an empirically observed ground velocity caused by a small earthquake on Γ , which can be actually observed by seismometers, approximates the kernel. Another tool to obtain the kernel is a straightforward calculation. Instead of solving eqs.(10a)–(10c), a propagator matrix method has widely been employed. In this method, only radial and stratified heterogeneity of the Earth is assumed (i.e., $\mathbf{C}(\mathbf{x}) = \mathbf{C}(R)$, where R is the distance from the center of the Earth, and \mathbf{C} is a step-wise function). Additionally, plane-wave decomposition, which is compatible with Snell's law, is considered; see the chapter 9 in [4] or 6.5 in [33] for details. These two methods are also applicable to inverse analyses shown in Section 3.2.

3.2 Kinematic Inverse Analysis of Fault Slip: $\mathbf{u} \mapsto \mathbf{m}$

After major earthquakes occur, seismologists investigate what happened on a fault by analyzing seismograms, which record the ground velocity $\partial_t \mathbf{u}(\mathbf{x}, t)$ for $\mathbf{x} \in \partial\Omega$. Thus the time-derivative of eq.(7) gives an inversion problem to obtain moment rate $\partial_{\tau} \mathbf{m}$ once $\partial_t \mathbf{u}^{\text{obs}}(\mathbf{x}, t)$ is observed. As with the previous subsection, this is a kinematic modeling of faulting. Effectively, the following equation is widely assumed:

$$\partial_t \mathbf{u}^{\text{obs}}(\mathbf{x}, t) = \int_{\Gamma} \partial_{\tau} \mathbf{m} * \nabla_{\xi} \mathbf{G} d\xi + \mathbf{e}(\mathbf{x}, t), \quad (13)$$

where an error vector \mathbf{e} is added because synthetic waveforms calculated via the integral on the right-hand side must not strictly agree with the observed ones owing to some errors in the observation system, modeling process, and/or uncertainty of the Green tensor. Discretized form of eq.(13) is reduced to

$$\partial_t u_n^{\text{obs}}(\mathbf{x}^i, t^j) = \partial_{\tau} m_{kl}(\xi^p, \tau^q) \partial_{\xi_l} G_{kn}(\mathbf{x}^i, \xi^p, t^j - \tau^q) \delta \xi \delta \tau + e_n(\mathbf{x}^i, t^j), \quad (14)$$

where i and j are up to the numbers of observation points and samples of time series, respectively; and p and q are up to P and Q , the numbers of spatial and temporal discretization for the source process, respectively. Using linear equation solvers, we obtain some approximated solutions that minimize the norm of \mathbf{e} (e.g., a (damped) least square solution[24]). However, P and Q are arbitrary, and the error reduces to an infinitesimal value as P and Q increase. Overfitted solutions in such a case are not robust, and we have to choose appropriate values of P and Q based on certain criteria. In many cases, Akaike's information criterion, which is equivalent to the principle of maximum entropy, is employed[1]. Moreover, the Bayesian information criterion has been employed to determine unknown hyperparameters that describe the smoothness of the solution on the basis of prior constraints from a physical point of view[2, 37]. More reviews on a practical procedure and results are found in [19], and a project to validate various schemes to solve this problem is on-going[26].

3.3 Inverse Analysis of Fault Dynamics: $\mathbf{m} \mapsto -\mathbf{T} = \mathbf{T}_0 - \mathbf{f}$

In seismology, traction and friction acting on fault surfaces are not directly observable. Given the inverted moment tensor \mathbf{m} , investigating the evolution of co-seismic traction $\mathbf{T}(\mathbf{x}, t)$ is a challenging problem. Substituting eq.(7) to eq.(2)–(4), we obtain a linear relationship between them as Γ :

$$\mathbf{T}(\mathbf{x}, t) = \mathfrak{T} \int_{\Gamma} \mathbf{m} * \nabla_{\xi} \mathbf{G} d\xi, \quad (15)$$

where the linear operator \mathfrak{T} maps any displacement field to shear traction perturbation on Γ resulting from the combination of eqs.(2)–(4). This equation and a relation $-\mathbf{T}(\mathbf{x}, t) = \mathbf{T}_0(\mathbf{x}) - \mathbf{f}(\mathbf{x}, t)$ from eq.(6b) enables the estimation of dynamic stress drop, temporal variation of the difference between initial traction \mathbf{T}_0 and friction \mathbf{f} on the fault. In other words, it is not possible to estimate their magnitude separately using only seismic data.

In general, after seismic inversion analyses to obtain the moment tensor, \mathbf{T} is inverted using an FDM[20, 28] or by assuming some characteristic form of the moment rate $\partial_{\tau} \mathbf{m}$ [36]. In principle, however, we can calculate the shear traction perturbation using eq.(15). This calculation is, in fact, not straightforward because the integration kernel $\mathfrak{T} \nabla_{\xi} \mathbf{G}(\mathbf{x}, \xi, t - \tau)$ has a hyper singularity for $\mathbf{x} \sim \xi$ as shown in

section 4; note that the integration on the right-hand side of eq.(15) is taken over Γ including the evaluation point \mathbf{x} of the left-hand side. If Ω is an infinite homogeneous isotropic medium and Γ is flat, it is represented by eq.(15) in the frequency-wavenumber domain according to Bouchon[9]:

$$\mathfrak{F}\mathbf{T}(\mathbf{k}, \omega) = \mathfrak{F}\mathbf{m}(\mathbf{k}, \omega)\mathfrak{F}(\mathfrak{T}\nabla_{\xi}\mathbf{G})(\mathbf{k}, \omega), \quad (16)$$

where Fourier transform with respect to space and time

$$\mathfrak{F}f(\mathbf{k}, \omega) = \int_{\mathbf{R}^1} \left\{ \int_{\Gamma} f(\mathbf{x}, t) e^{i\mathbf{k}\cdot\mathbf{x}} d\mathbf{x} \right\} e^{-i\omega t} dt$$

is applied. However, the spectrum of the kernel could diverge in the wavenumber domain due to the hyper-singularity. Indeed, the amplitude of the kernel $|\mathfrak{F}(\mathfrak{T}\nabla_{\xi}\mathbf{G})|$ is an increasing function of $|\mathbf{k}|$, such that an inverse Fourier transformation of (16) exists only when \mathbf{m} is sufficiently smooth. The difficulty due to the hyper-singularity retained in the spectral domain is reduced by regularizing the kernel in the time domain as discussed in Section 4.

3.4 Forward Analysis of Fault Dynamics: $-\mathbf{T} = \mathbf{T}_0 - \mathbf{f} \mapsto \mathbf{m}$

In mechanics, obtaining movements under given force and/or stress states is a forward problem. In our case, the fault slip is obtained after assuming the stress drop. This is quite a difficult problem because we cannot measure \mathbf{T}_0 or \mathbf{f} independently and seismologically. \mathbf{T}_0 is considered to be exceedingly heterogeneous on faults because Earth's crust (i.e., surroundings of faults) has multi-scale structures. Moreover, in general, \mathbf{f} non-linearly depends on the intrinsic state variable θ of the slipping surface[11, 29, 13, 5], normal stress \mathbf{N} , slip $[\mathbf{u}]$, and slip velocity $\partial_t[\mathbf{u}]$. Hence,

$$\mathbf{T}_0(\mathbf{x}) - \mathbf{f}(\theta, \mathbf{N}, [\mathbf{u}], \partial_t[\mathbf{u}]) = -\mathfrak{T} \int_{\Gamma} \mathbf{m} * \nabla_{\xi} \mathbf{G} d\xi \quad (17)$$

holds. Eq.(17) is a non-linear integro-differential equation of fault slip. To solve a discretized form of eq.(17), the Boundary Integral Equation Method (BIEM, or Boundary Element Method, BEM), which is widely employed for physical modeling, is used; see Ando[7] for its history and procedures. This is equivalent to solving eqs.(5a)–(5c) with eq.(6b).

In many fields, including acoustics and electromagnetics, such an integral is sometimes considered in the frequency domain. Analyses in the frequency domain are powerful tools when the focus is on phenomena considering a certain frequency. However, no specific frequency can be considered in fault mechanics. Instead, we consider fracture criteria that must hold at every moment, such that eq.(17) can be solved in the time domain. Under the maximum stress criterion, $|\mathbf{f}| \leq f_s$ must hold at any given time, where f_s is the maximum static friction. Under the Griffith frac-

ture criterion, the work rate $G = \int_{\Gamma} \mathbf{f} \cdot [\dot{\mathbf{u}}] d\boldsymbol{\xi}$ must be balanced with the fracture energy G_C at any given time.

Friction \mathbf{f} has been investigated throughout laboratory experiments with various rocks. Recent reviews and advances on very-low slip velocity less than 10^{-2} m/s have been concentrated on the temporal evolution and physical background of friction [11, 29, 13]. In fact, co-seismic slip velocity is typically within the range of ~ 1 -10 m/s, where no consensus on a unified friction law is reached. The slip-weakening law, which was originally introduced in a numerical modeling[18] and consequently confirmed in a laboratory[30], is widely employed in simulations:

$$\frac{|\mathbf{f}|}{|\mathbf{N}|} = (\mu_s - \mu_d) \phi\left(\frac{D}{D_c}\right) + \mu_d, \quad (18)$$

where μ_s and μ_d are the static and dynamic friction coefficients, respectively. $D = |[\mathbf{u}]|$ is slip distance, and $\phi(x)$ is a continuous and monotonically decreasing function from $\phi(0) = 1$ to $\phi(x)|_{1 \leq x} = 0$. In many studies, $\phi(x) = (1-x)H(1-x)$, where $H(\cdot)$ is the Heaviside function, is employed for simplicity. The characteristic slip-weakening distance D_c is a critical parameter describing the law. In slip-weakening friction, the path-independent integral that should be balanced with the fracture energy is represented as follows[31]:

$$J - \mu_d |\mathbf{N}| D_c = \int_0^{D_c} (|\mathbf{f}| - \mu_d |\mathbf{N}|) dD,$$

where the left-hand side is path-independent. On the other hand, other friction laws for the co-seismic slip velocity range has been suggested. For example, a velocity- and state-dependent friction law based on thermodynamics on the slipping plane

$$\frac{|\mathbf{f}|}{|\mathbf{N}|} = \mu_s + \alpha \frac{V}{V + V_c} - \beta \frac{\theta}{\theta + V_c}, \quad (19)$$

$$\partial_t \theta = \frac{V - \theta}{D_c / V_c}, \quad (20)$$

has been employed[5], where $V = |\partial_t[\mathbf{u}]|$, and α, β , and V_c are positive constants. Using this law, an observed pulse-like rupture, where the duration of slip is significantly shorter than that of the entire faulting process[14], can be reproduced.

4 Summary and Discussion

As shown in the previous section, the representation theorem (7) reveals relationships among seismic wavefield, slip, and stress drop on the fault and enables their analysis; see summary in Table.1. In this section, we discuss a difficulty experienced during the execution of the analyses.

Table 1 Summary of forward/inverse analyses of fault kinematics/dynamics.

		Forward	Inverse
Kinematics	eq.	(7)	(13)
	based on	assumed fault slip \mathbf{u}	observed seismic wavefield \mathbf{u}
	solving for	seismic wavefield \mathbf{u}	fault slip \mathbf{u}
Dynamics	eq.	(17)	(15)
	based on	assumed stress drop $-\mathbf{T}$	estimated fault slip \mathbf{u}
	solving for	fault slip \mathbf{u}	stress drop $-\mathbf{T}$

In reality, calculations using these equations are not archived literally because of the singularity of the integration kernel $\nabla_{\xi}\mathbf{G}$. An asymptotic representation of $\nabla_{\xi}\mathbf{G}$ is $\sim \partial_t\delta(t-r/v)/r$ for the far field (i.e., larger r) and $\sim \delta(t-r/v)/r^2$ for the near field (i.e., smaller r)[3, 4], where $r = |\mathbf{x} - \xi|$ is distance between the source and the observation point, and v is the propagation speed of the wave.

In cases of the kinematic modeling in Section 3.1 and Section 3.2, the singularity does not matter. For eqs.(7) and (13), the displacement field is observed at the far field in many cases. Therefore, the singularity of $\sim \partial_t\delta(t-r/v)/r$ dominates, and the denominator is non-singular in the far field. The numerator, Dirac's delta function, is unrealistic for modeling seismic waves because intrinsic attenuation of Earth's interior prevents the propagation of high-frequency components of waves towards the far field. Hence, we should consider the effective application of some low-pass filter $F(t)$ to the kernel[38]:

$$\partial_t\mathbf{u}^{\text{obs}} \sim \int_{\Gamma} \partial_t\mathbf{m} * (F * \nabla_{\xi}\mathbf{G}) d\xi + \mathbf{e}.$$

As a result, the asymptotic form of the kernel $\sim \partial_tF(t-r/v)/r$ is finite and manageable in numerical schemes. Conventionally, F has been modeled as $|\mathfrak{F}F(\omega)| \sim e^{-\omega/Q}$ in the frequency domain, where the dimensionless parameter Q is the fractional energy loss per cycle; see section 5.5 in [4] or 6.6 in [33]. Needless to say, the low-pass filtered kernel lacks shorter wavelength components. Thus, the resolution of the solution is reduced and depends on the characteristics of the attenuation. Effectively, the power of the filter is reduced by more than ~ 1 Hz in the frequency domain, which is equivalent to smaller than ~ 6 km in space because a typical dilatational wave speed is ~ 6 km/s in Earth's crust. The lack of resolution affects not only the fault slip inversion but also estimations of co-seismic potential energy release and kinetic energy radiation[15], which have been controversial in seismology. Given the empirical power spectral density of slip distributions and theoretical consideration, estimation of the energy may become more difficult than that of slip[15].

The situation is more severe in the mechanical modeling in Section 3.3 and Section 3.4 because the near-field (i.e., $\mathbf{x} \sim \xi$) traction perturbation must be considered for eqs.(15) and (17). Aggravating the situation, the operator \mathfrak{T} consists of the first-order derivative, such that the singularity of $\mathfrak{T}(\nabla_{\xi}\mathbf{G}) \sim \delta(t-r/v)/r^3$ becomes dominant. The regularization of the hyper-singular integrals with integrations by

parts is a method for solving this difficulty. For an infinite homogeneous isotropic medium (i.e., Ω corresponds to \mathbb{R}^3 , and $C(\mathbf{x})$ is constant), Tada derived a regularized kernel of displacement and traction perturbation for a quadrantal fault[34] and a triangular fault[35]. In this manner, we can analyze the above integral equations with a numerically modeled fault surface that consists of polygons. Moreover, computational costs to treat Tada's regularized kernel has been dramatically reduced even with a free surface[6, 7]. Hence, the inverse modeling of co-seismic traction perturbation in Section 3.3 via eq.(15) will be used more actively as in [17] while the forward modeling in Section 3.4 with non-planar faults have already been applied in a homogeneous full-space[8] and a half-space[17, 6]. In addition, applications of regularized integral equations to heterogeneous elastic 2-D media are developing (e.g., anti-plane faulting in two-welded half spaces[16], and piecewise-homogeneous medium[22]). Because surroundings of faults are generally heterogeneous, the focus of future researches will be on numerical schemes to treat interactions between such media and also dynamic faulting processes in the 3-D domain.

Acknowledgements The author is grateful to T. Yamaguchi and T. Kusakabe for helpful discussions. Comments from a reviewer contributes to improve the manuscript. This is a post-peer-review, pre-copyedit version of an article published in van Meurs, P. *et al.* (eds) *Mathematical Analysis of Continuum Mechanics and Industrial Applications II. CoMFoSI6*. Mathematics for Industry, vol 30. Springer, Singapore. The final authenticated version is available online at: http://dx.doi.org/10.1007/978-981-10-6283-4_9.

References

1. Akaike, H., On entropy maximization principle, in *Application of Statistics* (1977) pp.27–41, ed. Krishnaiah, P.R., North-Holland, Amsterdam.
2. Akaike, H., Likelihood and the Bayes procedure, in *Bayesian Statistics* (1980) pp.143–166, eds. Bernardo, J.M., DeGroot, M.H., Lindley, D.V. & Smith, A.F.M., University Press, Valencia, Spain.
3. Aki, K. & P.G. Richards, Quantitative seismology, 1st ed. (1980), Freeman.
4. Aki, K. & P.G. Richards, Quantitative seismology, 2nd ed. (2002), University Science Books.
5. Ampuero, J.-P. & Y. Ben-Zion, Cracks, pulses and macroscopic asymmetry of dynamic rupture on a bimaterial interface with velocity-weakening friction, *Geophys. J. Int.* (2008) **173**, 674–692.
6. Ando, R., Fast domain partitioning method for dynamic boundary integral equations applicable to non-planar faults dipping in 3-D elastic half-space, *Geophys. J. Int.*, (2016) **207**, 833–847.
7. Ando R., On Applications of Fast Domain Partitioning Method to Earthquake Simulations with Spatiotemporal Boundary Integral Equation Method. In: van Meurs P., Kimura M., Notsu H. (eds) *Mathematical Analysis of Continuum Mechanics and Industrial Applications II. CoMFoSI6*. Mathematics for Industry, vol 30 (2018). Springer, Singapore.
8. Aochi, H., E. Fukuyama & M. Matsu'ura, Spontaneous Rupture Propagation on a Non-planar Fault in 3-D Elastic Medium, *Pure Appl. Geophys.* (2000) **157**, 2003–2027.
9. Bouchon, M., The state of stress on some faults of the San Andreas system as inferred from near-field strong motion data, *J. Geophys. Res.* (1997) **102**(B6) 11,731–11,744.
10. Burridge, R., & L. Knopoff, Body force equivalents for seismic dislocations, *Bull. Seism. Soc. Am.* (1964) **54**(6) 1875–1888.

11. Dieterich, J.H., Applications of rate- and state-dependent friction to models of fault slip and earthquake occurrence, in *Treatise on Geophysics, in Earthquake Seismology* (2007) **4**, pp.107–129, ed. Kanamori, H. (Series Editor), Elsevier, Amsterdam.
12. Haskell, N.A., Total energy and energy spectral density of elastic wave radiation from propagating faults, *Bull. Seism. Soc. Am.* (1964) **54**(6) 1811–1841.
13. Hatano, T., Friction laws from dimensional-analysis point of view, *Geophys. J. Int.* (2015) **202**, 2159–2162.
14. Heaton, T.H., Evidence for and implications of self-healing pulses of slip in earthquake rupture, *Phys. Earth Planet. Int.* (1990) **64**, 1–20.
15. Hirano, S. & Y. Yagi, Dependence of seismic and radiated energy on shorter wavelength components, *Geophys. J. Int.*, **209**(3) 1585–1592.
16. Hirano, S. & T. Yamashita, Dynamic antiplane rupture propagation crossing a material interface: modelling with BIEM, *Geophys. J. Int.* (2015) **200**(2) 1222–1235.
17. Hok, S. & E. Fukuyama, A new BIEM for rupture dynamics in half-space and its application to the 2008 Iwate-Miyagi Nairiku earthquake, *Geophys. J. Int.* (2011) **184**, 301–324.
18. Ida, Y., Cohesive force across the tip of a longitudinal-shear crack and Griffith’s specific surface energy, *J. Geophys. Res.* (1972) **77**(20) 3796–3805.
19. Ide, S., Slip inversion, in *Treatise on Geophysics, in Earthquake Seismology* (2007) **4**, pp.193–224, ed. Kanamori, H. (Series Editor), Elsevier.
20. Ide, S. & M. Takeo, Determination of constitutive relations of fault slip based on seismic wave analysis, *J. Geophys. Res.* (1997) **102**(B12) 27,379–27,391.
21. Irikura, K., Prediction of strong acceleration motion using empirical Green’s function, *Proc. 7th Japan Earthq. Eng. Symp.* (1986) 151–156.
22. Kame, N. & T. Kusakabe, Proposal of Extended Boundary Integral Equation Method for Rupture Dynamics Interacting With Medium Interfaces, *J. App. Mech.* (2012) **79**(3) 031017.
23. Kaneko, Y. & P.M. Shearer, Seismic source spectra and estimated stress drop derived from cohesive-zone models of circular subshear rupture, *Geophys. J. Int.* (2014) **197**(2) 1002–1015.
24. Kikuchi, M. & H. Kanamori, Inversion of complex body waves—III, *Bull. Seism. Soc. Am.* (1991) **81**, 2335–2350.
25. Madariaga, R., High-frequency radiation from crack (stress drop) models of earthquake faulting, *Geophys. J. R. astr. Soc.* (1977) **51**, 625–651.
26. Mai, P.M., D. Schorlemmer, M. Page, J-P. Ampuero, K. Asano, M. Causse, S. Custodio, W. Fan, G. Festa, M. Galis, F. Galovic, W. Imperatori, M. Käser, D. Malyskyy, R. Okuwaki, F. Pollitz, L. Passone, H. Razafindrakoto, H. Sekiguchi, S. Song, S. Somala, K. Thingbaijam, C. Twardzik, M. van Driel, J. Vyas, R. Wang, Y. Yagi, & O. Zielke, The earthquake-source inversion validation (SIV) project, *Seism. Res. Lett.* (2016), **87**(3) 690–708.
27. Maruyama, T., On the force equivalents of dynamical elastic dislocations with reference to the earthquake mechanism, *Bull. Earthq. Res. Inst.* (1963) **41**, 467–486.
28. Mikumo, T., K.B. Olsen, E. Fukuyama & Y. Yagi, Stress-breakdown time and slip-weakening distance inferred from slip-velocity functions on earthquake faults, *Bull. Seism. Soc. Am.* (2003) **93**(1) 264–282.
29. Nagata, K., M. Nakatani & S. Yoshida, A revised rate- and state-dependent friction law obtained by constraining constitutive and evolution laws separately with laboratory data, *J. Geophys. Res.* (2012) **117**, B02314.
30. Ohnaka, M. & T. Yamashita, A cohesive zone model for dynamic shear faulting based on experimentally inferred constitutive relation and strong motion source parameters, *J. Geophys. Res.* (1989) **94**(B4) 4089–4104.
31. Palmer, A.C. & J.R. Rice, The growth of slip surfaces in the progressive failure of over-consolidated clay, *Proc. Roy. Soc. Lond. A.* (1973) **332**, 527–548.
32. Sato, T. & T. Hirasawa, Body wave spectra from propagating shear cracks, *J. Phys. Earth.* (1973) **21**, 415–431.
33. Shearer, P.M., Introduction to seismology, 2nd ed. (2009), Cambridge university press.
34. Tada, T., Displacement and stress Green’s functions for a constant slip-rate on a quadrantal fault, *Geophys. J. Int.* (2005) **162**, 1007–1023.

35. Tada, T., Stress Green's functions for a constant slip rate on a triangular fault, *Geophys. J. Int.* (2006) **164**, 653–669.
36. Tinti, E., E. Fukuyama, A. Piatanesi & M. Cocco, A kinematic source-time function compatible with earthquake dynamics, *Bull. Seism. Soc. Am.* (2005) **95**(4) 1211–1223.
37. Yabuki, T. & M. Matsu'ura, Geodetic data inversion using a Bayesian information criterion for spatial distribution of fault slip, *Geophys. J. Int.* (1992) **109**(2) 363–375.
38. Yagi, Y. & Y. Fukahata, Introduction of uncertainty of Green's function into waveform inversion for seismic source processes, *Geophys. J. Int.* (2011) **186**, 711–720.